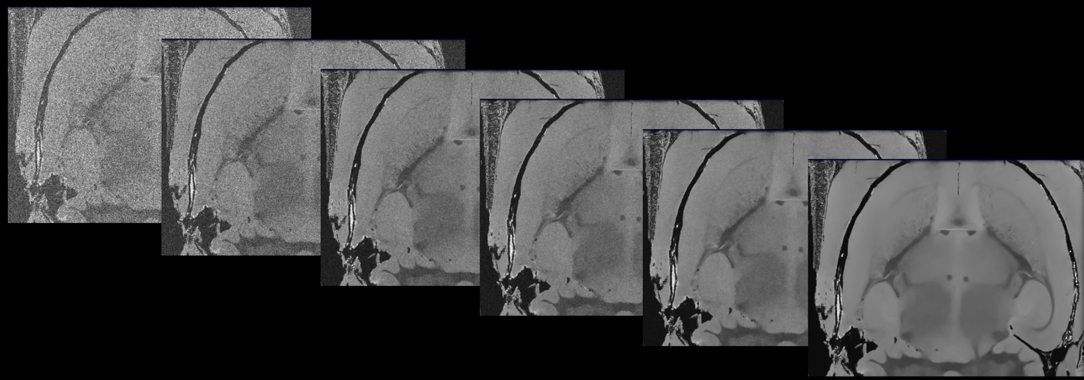

PRECLINICAL IMAGING

Evaluation of ParaVision 360 Smart Noise Reduction Algorithm for Structural MR Imaging

Jan Klohs, Michael Herbst, Martin Haas, Thomas Basse-Luesebrink
Bruker BioSpin GmbH & Co. KG

Innovation with Integrity

Introduction

Magnetic resonance imaging (MRI) is one of the most widely used imaging modalities in preclinical research as it provides multiparametric information about tissues and organs in a non-invasive way. The small dimensions of the animal organism require high spatial resolution which in turn translates into high demands on the signal-to-noise ratio (SNR).

MRI systems are designed to obtain images with high SNR by using magnets operating at high and ultra-high fields and use dedicated radiofrequency coils and scanner electronics. However, the quality of MR images can be affected by thermal object and receiver noise governed by individual hardware settings, type of tissue imaged, and sequence parameters. Noisy images may result from experimental conditions when: (i) small voxel volumes are used to spatially resolve specific structures (ii) averaging may either not be desirable or be practical, (iii) methods that require signal attenuation for contrast generation like diffusion MRI and relaxometry, or (iv) parallel imaging techniques are applied [Macovski 1996; Aja-Fernández 2014].

Images with high noise levels may pose an obstacle in visual interpretation and may result in a sensitivity that is too low to detect small signal changes, such as in functional MR experiments. In addition, processing techniques such as registration or conducting quantitative MRI e.g. tensor estimation in diffusion tensor imaging may be more challenging [Huang 2004]. Thus, denoising algorithms to improve both qualitative and quantitative measures of noisy images are increasingly exploited in the MRI field [Mishro 2022].

Smart Noise Reduction

With ParaVision 360 V3.6, Bruker introduced Smart Noise Reduction, a novel image reconstruction procedure to reduce and remove noise from MR images. The Smart Noise Reduction image reconstruction procedure is based on residual convolutional neural networks that have learned the structure of noise, which can be removed from the original data. The networks were trained using supervised learning, excluding any generative approach. A data-consistency factor allows for an adjustable denoising level, avoiding over-smoothing and maintaining image contrast. Using this data-consistency in combination with an iterative denoising (Pre-Denoising) technique, the quality of the final images can be substantially improved.

The Smart Noise Reduction contains three neural networks differing in structure and size for the denoising procedure. While small network size (network Quick) has the fastest processing times, the more powerful structures (networks Strong and Large) reduce the requirements regarding noise characteristics. Exemplary denoising results of these three networks are shown in **Fig 1**. To demonstrate the effect of denoising with the different networks, a denoised 3D dataset was taken as reference. Two levels of simulated noise (Standard deviation 0.05 and 0.1) were added to the reference image which were then subsequently used as an input for the three denoising networks (Quick, Strong, and Large). All datasets were denoised with 50% pre-denoising and a denoising level of 100%.

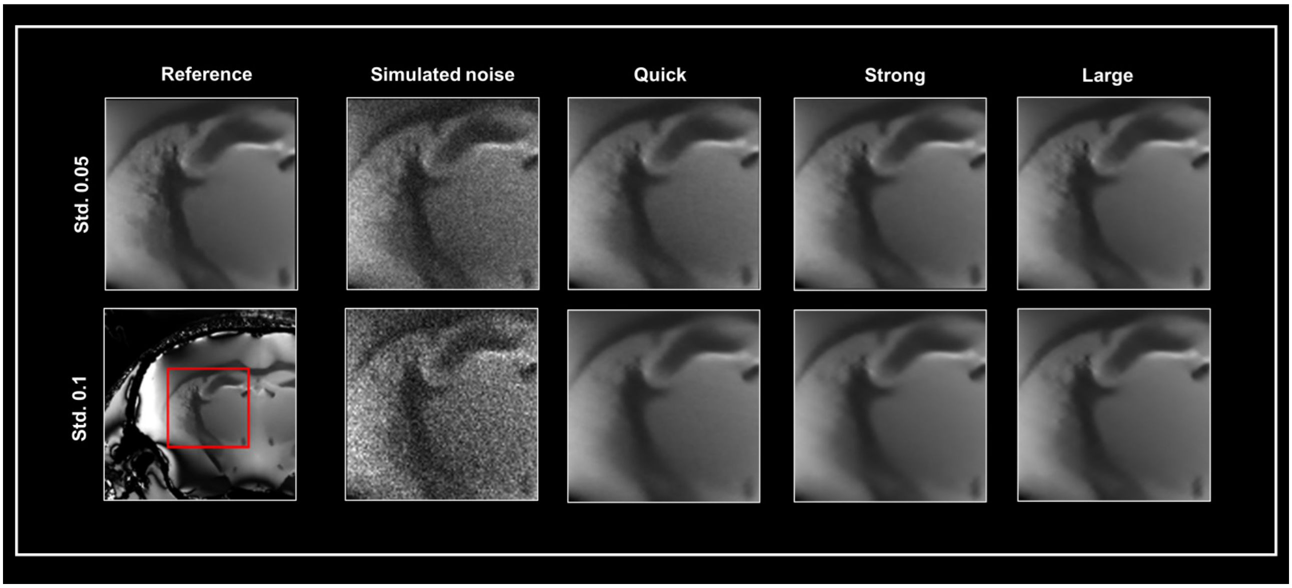

Figure 1: Smart Noise Reduction using different neuronal networks. A denoised 3D dataset was taken as ground truth (Reference) to which two varying levels of simulated noise were added, i.e. standard deviation (Std.) 0.05 and 0.1, respectively. Noisy data were subsequently reconstructed with the Quick, Strong, and Large networks. All data were denoised with a 100% denoising level and 50% pre-denoising. The area shown in the red box was selected for the similarity metrics in Table 1.

Performance Evaluation

The main challenge of performing denoising on structural MR images consists in reducing the amount of noise, while preserving the details, the edges, and in general the small structures that could be crucial for interpretation and analysis of the image. Moreover, the procedure should not introduce image artifacts or add features that are not actually present in the subject.

To quantify the quality of the reconstructed images shown in **Fig. 1**, the Peak Signal to Noise Ratio (PSNR) and Structural SIMilarity (SSIM) index between the reference image and the data reconstructed with the three different networks were calculated (shown in **Table 1**). The selected area for the analysis is highlighted in **Fig. 1**. While implementation of the Large network provides the best performance, also the fast reconstruction with the Quick and Strong networks yield images of good quality.

Noise	Metric	Quick	Strong	Large
Std. 0.05	PSNR	37.272	38.592	39.152
	SSIM	0.9439	0.9657	0.9711
Std. 0.1	PSNR	34.239	35.380	35.939
	SSIM	0.9332	0.9483	0.9531

Table 1: Quantitative comparison of performance of three neuronal networks for Smart Noise Reduction. For the SSIM index 0 indicates no similarity and 1 indicates perfect similarity. Bold indicates the best performing network.

In addition to the choice of network, it is also possible to select the denoising level. **Fig. 2A** demonstrates the effect of applying different levels of denoising for image reconstruction. Mouse brain data was acquired *ex vivo*, the original data was reconstructed without any denoising as well as with increasing denoising levels (70-100%). Increasing denoising levels yield images where noise is progressively removed. Importantly, no artifacts were introduced during the procedure. Computing a difference image between the source and 70% denoised images demonstrated that only noise is selectively removed. If the original signal at the edges of the images is lower due i.e. to bandwidth selection, high denoising levels (i.e. 90 and 100%) can lead to a blurry appearance of edges. Thus, the optimal denoising level, providing a trade-off between efficient noise removal and edge blurring, needs to be established individually for each data set or at least for each application protocol.

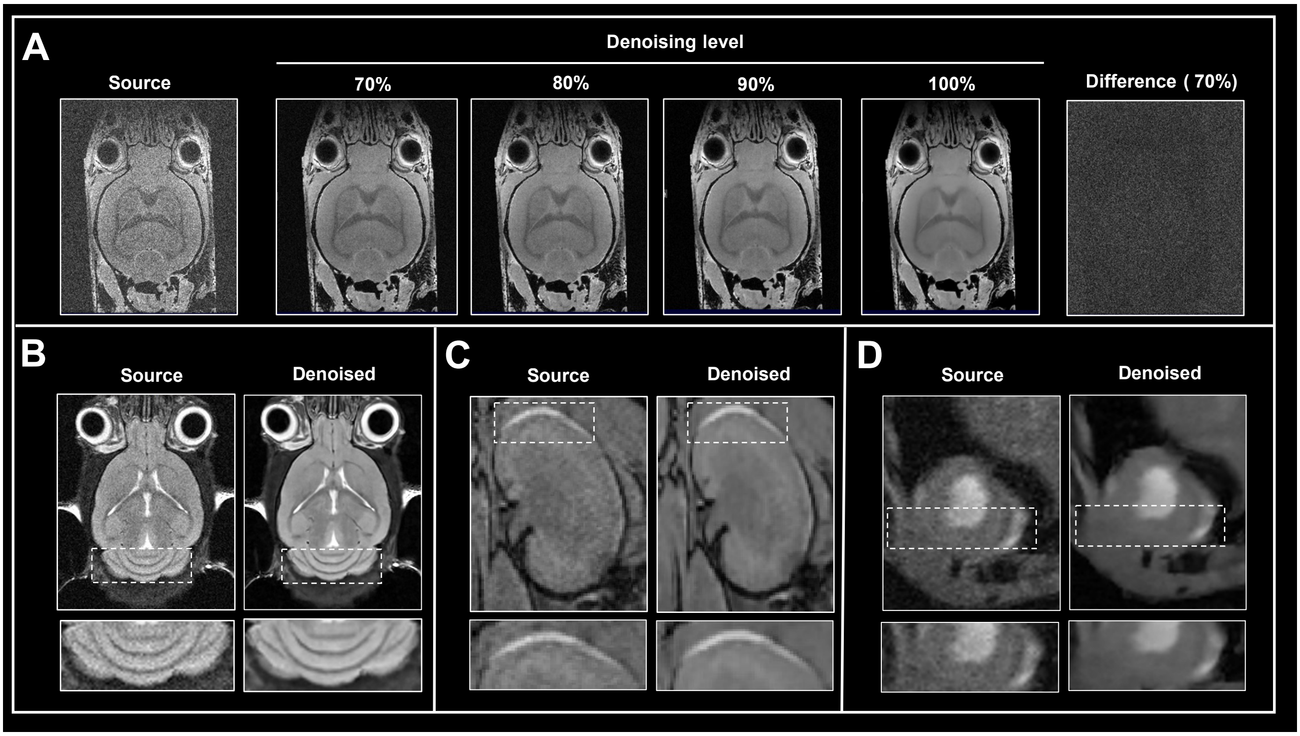

Figure 2: The effect of image denoising on image quality. A) Applying increasing levels of denoising. Shown are axial images of a 3D T1-weighted FLASH *ex vivo* data of a fixed mouse head acquired at 9.4 Tesla without (Source) and different levels (70-100%) of denoising. A difference image between the source and 70% denoised images was computed. B)-D) Comparison of *in vivo* images reconstructed with no denoising and with 70% denoising. B) Coronal T2-weighted TurboRARE images of a mouse brain acquired at 3 Tesla. C) Coronal 3D FISP images of mouse kidney acquired at 7 Tesla. D) Short axis view of a mouse heart acquired with a flow-compensated triggered FLASH sequence at 9.4 Tesla. For different data, either no denoising (Source) or denoising using individual networks and a pre-denoising of 50% was applied (Denoised).

The utility of Smart Noise Reduction was demonstrated on *in vivo* mouse data of different organs acquired at different magnetic field strengths (**Fig. 2B-D**). Compared to the reference images of the brain, kidney, and heart, reconstruction with 70% denoising provided images with significantly reduced noise and enhanced appearance of anatomical details and edges.

To test the performance of the denoising algorithm with images of different levels of tissue contrast, *ex vivo* data of a fixed mouse brain was acquired with a nominal voxel size of 55 x 55 x 800 µm^3 at 3 Tesla, either with no averaging, 4, or 15 averages (**Fig. 3**). This corresponds to a contrast-to-noise ratio between the corpus callosum and cortex of 2.47±0.45, 4.59±0.01, and 12.03±0.81, respectively. Images were reconstructed without and with 70% and 100% denoising. Given the relatively high resolution, the image without averaging exhibits low tissue contrast and suffers from noise which can be mitigated by using averaging during acquisition or using denoising during image reconstruction. However, the comparison of denoised images acquired with different numbers of averages reveals that denoising can amplify spurious contrast in cases of low tissue contrast i.e. no averaging (**Fig. 3**, arrow).

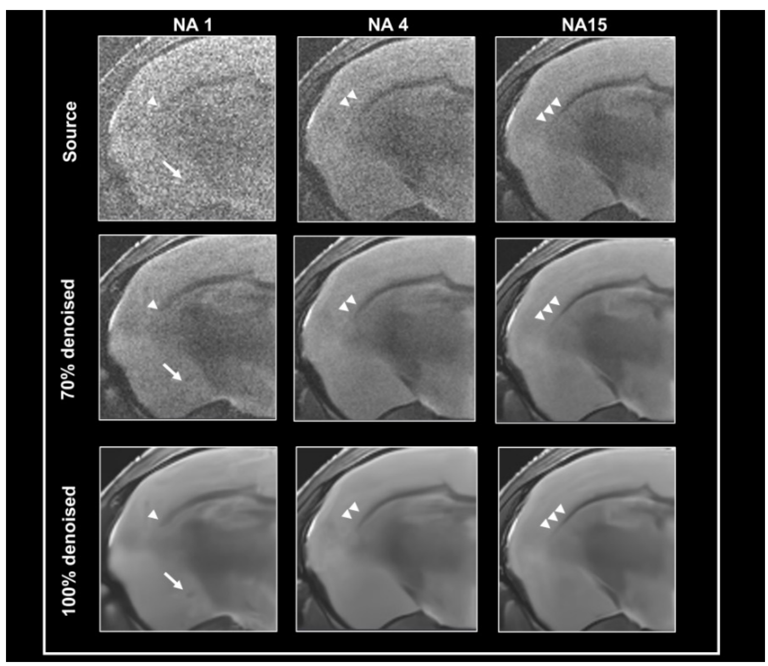

Figure 3: Denoising images with low tissue contrast. A) Axial T2-weighted TurboRARE images of a fixed mouse head were acquired at 3 Tesla with 1, 4 and 15 number of averages (NA), respectively. Images have a nominal voxel resolution of 55 x 55 x 800 µm3. Image reconstruction was performed without (Source) and with 70% and 100% denoising. Each denoised image was reconstructed with a network Strong and a pre-denoising of 50% was applied. The arrows point to a structure in the NA1 images, that is faintly visible in the image that has not been denoised and that becomes more apparent with increasing denoising. The arrowheads point to the corpus callosum which becomes more visible. Resolution of fine structure requires high tissue contrast with averaging.

This structure that is faintly visible in the noisy image without using denoising but is not well distinguishable from the surrounding tissue is enhanced by increasing levels of denoising. Comparison between images using different levels of averaging demonstrates that with denoising the corpus callosum becomes more visible (**Fig. 3**, arrowheads). To resolve the fine structure of the extent of the corpus callosum, however, requires high tissue contrast with averaging. If this is given, denoising enhances the visualization.

Faster Imaging

The acquisition of MRI data is an inherently slow process and acquisition times increase with higher spatial resolution, when large volumetric coverage is required, and/or when multiple contrast images or quantitative data sets are collected. Obtaining high SNR data in reasonable acquisition time is highly desirable. Here, we showcase the use of Smart Noise Reduction for denoising of fast structural brain scans.

Fig. 4 shows examples of *ex vivo* brain scans of different contrasts and orientations acquired in under 5 minutes. The data was acquired at instruments operating at 3, 7, and 9.4 Tesla. To achieve the desired short acquisition time, standard protocols prepared for each system were modified by removing averaging (**Fig. 4A-C**) This translated into 7-15 faster acquisition times compared to the original protocols. However, given the chosen resolution, no averaging resulted in noisy images. Reconstructing the acquired data with the denoising algorithm successfully removed noise from images and yielded images of high quality.

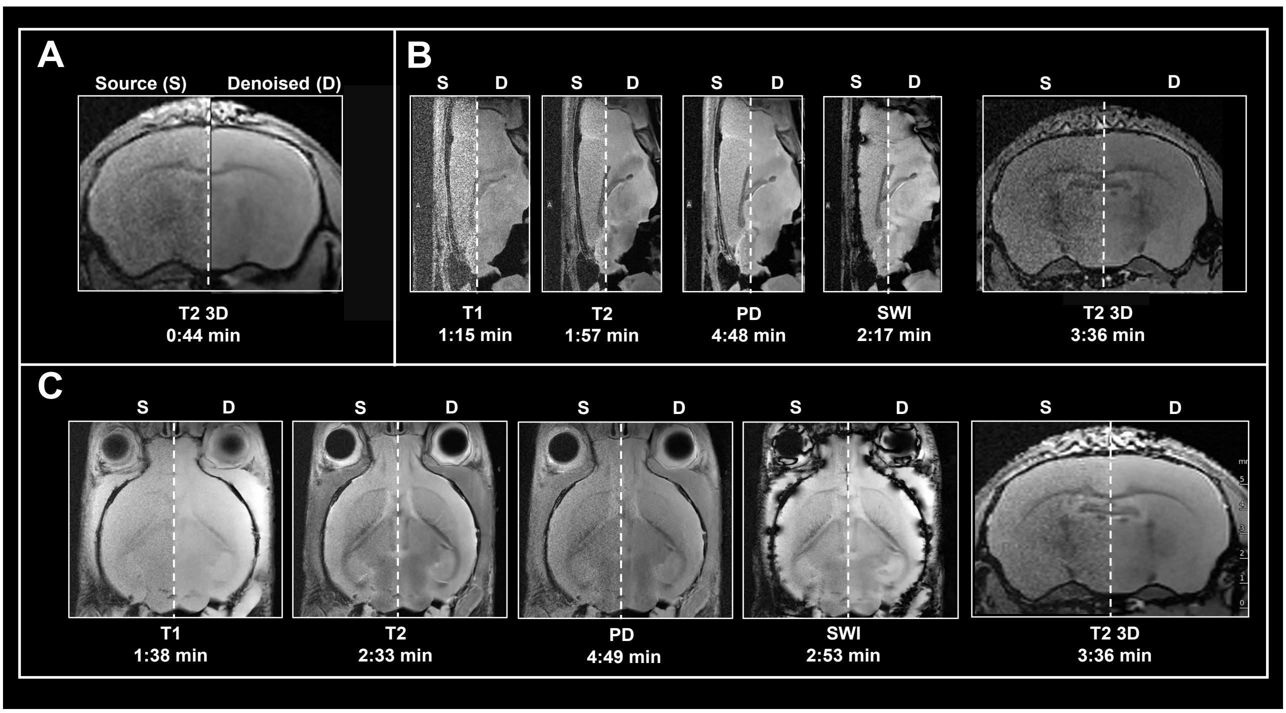

Figure 4: Examples of fast brain scans. *Ex vivo* data of a fixed mouse head acquired with different image contrasts, geometries and orientations. Data were acquired at A) 3 Tesla, B) 7 Tesla, and C) 9.4 Tesla. Images were reconstructed with no denoising (Source) and with a network Strong and applying 50% pre-denoising and a denoising level of 70% (Denoised).

Several approaches to speed up MRI acquisitions by exploiting temporal or spatiotemporal redundancy of the images have been introduced in the literature [Pruessmann 1999, Griswold 2002]. Techniques like parallel imaging produce structured noise in the reconstructed image because of the decreased data sampling and noise amplification caused by the parallel reconstruction algorithm [Aja-Fernández 2014]. *Ex vivo* brain data were acquired with either partial Fourier or the multi-coil generalized auto-calibrating partial parallel acquisition (GRAPPA) technique (**Fig. 5**). Data acquired without acceleration served as a reference. Acceleration translated into an up to 3-fold reduction in acquisition times compared to the protocol when no averaging was used.

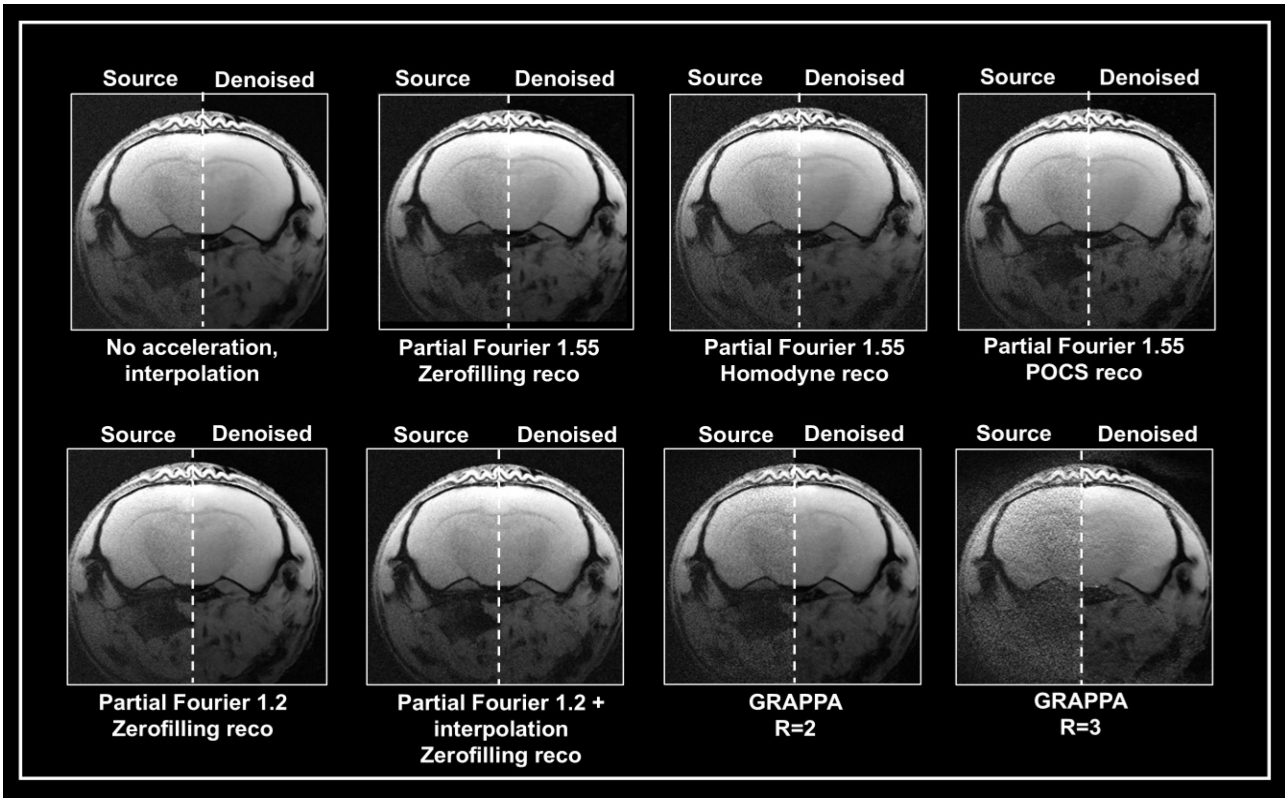

Figure 5: Denoising of accelerated brain data. *Ex vivo* T1-weighted FLASH data of a fixed mouse head were acquired at 9.4 Tesla. Data were either acquired with no acceleration, with partial Fourier (in Read), partial Fourier and interpolation (1.35 in Read and Phase), or with multi-coil parallel imaging technique GRAPPA. For GRAPPA, an acceleration factor (R) of 2 and 3 was chosen, respectively. Partial Fourier images were reconstructed either with zerofilling, homodyne, or POCS, as indicated. All images are shown with no denoising (Source) and after denoising (Denoised) with a Strong network, applying a pre-denoising level of 50% and denoising level of 70%.

A denoising of level of 70% resulted in more residual noise in data acquired with a partial Fourier 1.55 as compared to data acquired without acceleration. The effect was strongest in homodyne reconstructed data and lower in zerofilled data. Moreover, denoising of these accelerated datasets resulted in image blurring which was also strongest in homodyne reconstructed images and lowest in images reconstructed with zerofilling. Acquiring images with partial Fourier 1.2 resulted in less residual noise and normal image appearance when denoised with 70%. Denoising, however, was not effective when combining a partial Fourier with interpolation (1.35 in Read and Phase) with both the source and the denoised image having similar appearance.

Grappa acceleration resulted in noisier images than in acquisition with partial Fourier. Reconstructing the acquired data with the denoising algorithm successfully removed noise from the GRAPPA image acquired with an acceleration factor 2. However, in the image acquired with an acceleration factor 3, the noise is not completely removed. Moreover, reconstruction artifacts and loss of tissue contrast unrelated to the denoising reconstruction are apparent. This shows that the algorithm may not be able to deal with data that has a noise characteristic that differs from the noise that the networks have been trained with (i.e. without acceleration and interpolation). However, the result depends on the chosen acquisition and reconstruction parameters.

Taken together, denoising may improve images where SNR is reduced by applying faster imaging protocols. The overall decrease of acquisition time that can be achieved by adaptation of imaging protocols can significantly reduce the exposure time of animals in the instrument and can thus be used for the refinement of the method. In addition, it allows either to obtain additional read-outs during an MRI examination or to enable higher throughput for research.

Boosting the Resolution of Images per Unit Time

High-resolution MRI provides detailed structures in tissue and organs and can help to detect abnormalities like lesions or tumors. High-resolution structural MRI scans require long image acquisition times to overcome the inherit low SNR. Here we demonstrate how the use of Smart Noise Reduction can be used to shorten these acquisition times while maintaining the necessary image quality.

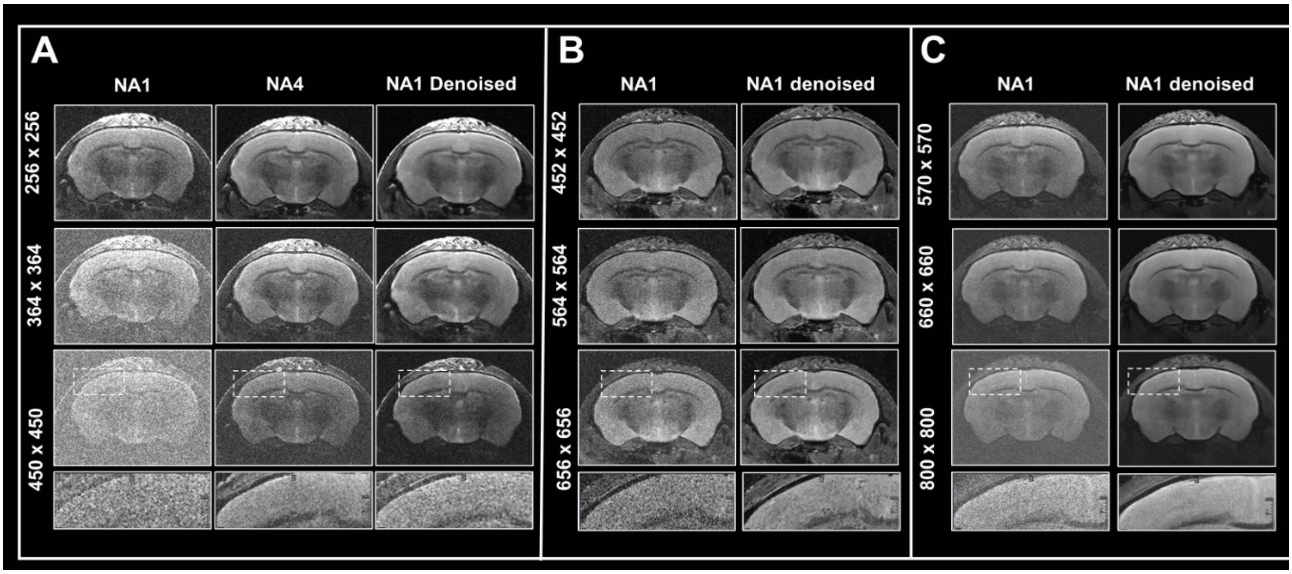

Figure 6: Boosting resolution. *Ex vivo* T2-weighted TurboRARE data of a fixed mouse head acquired at A) 3 Tesla, B) 7 Tesla, and C) 9.4 Tesla. All images were acquired with 0.8 mm (A) and 0.7 mm (B, C) slice thickness and with a field-of-view of 20 x 20 mm2 and the given matrix size using either no averaging or acquiring 4 averages. Images were reconstructed with no denoising (NA1 and NA4), or after denoising (NA1 Denoised) using a network Large, applying a pre-denoising level of 50% and denoising level of 70%.

In **Fig. 6**, axial T2-weighted TurboRARE images of a fixed mouse head acquired at different field strengths are compared. Images were acquired with a fixed field-of-view of 20 x 20 mm^2, with 0.8 mm (3 Tesla) and 0.7 mm (7 and 9.4 Tesla) thick slices and with varying matrix sizes to yield images with different spatial resolutions. In particular, the matrix sizes were increased by up to a factor of 1.8, 2.6 and 3.1 (vs a matrix size of 256 of the reference protocols) for images acquired at 3, 7 and 9.4 Tesla, respectively. These resolution increases result in a concomitant loss in SNR for each image. The loss in SNR can be compensated by using averaging and thus additional data was acquired with four averages. The comparison of non-denoised averaged images with single averaged images that were denoised reveals that denoising mitigates increased image noise at higher resolutions and produces images of similar quality to that of images acquired with averaging. The gains in image quality by denoising are higher with data acquired at 3 Tesla where increasing the resolution yields images that are more difficult to interpret compared to data acquired at 7 and 9.4 Tesla where SNR is inherently higher. Nevertheless, images acquired at 7 and 9.4 Tesla benefit substantially from denoising during reconstruction, as the intrinsic higher SNR of these images can be invested into selecting smaller voxel dimensions. Thus, taken together denoising enables to choose higher resolutions within a given unit time as it reduces the need for averaging. This can also be practical in cases where averaging may either not be desirable or practical.

Conclusion

Smart Noise Reduction allows to efficiently remove noise from structural images and thus to improve image quality of acquired data. With denoising levels and network choices, the user has options to optimize denoising results to their applications and needs. Noisy images are improved in cases where SNR is limited e.g. images obtained at low field strengths, when optimal coils are not available, or when averaging is not practicable or desired. In cases where SNR is sufficient, denoising can be used to boost resolution per unit time or chosen to make acquisitions faster.

Abbreviations

CNR = contrast-to-noise ratio; FISP = fast imaging with steady state precession; FLASH = fast low angle shot; GRAPPA = generalized autocalibrating partial parallel acquisition; MRI = magnetic resonance imaging; NA = number of averages; PSNR = peak signal to noise ratio; RARE = rapid acquisition with relaxation enhancement; SNR = signal-to-noise ratio; SSIM = structural similarity; SWI = susceptibility weighted imaging

References

Aja-Fernández S, Vegas-Sánchez-Ferrero G, Tristán-Vega A. Noise estimation in parallel MRI: GRAPPA and SENSE. Magn Reson Imaging. 2014 Apr;32(3):281-90. doi: 10.1016/j.mri.2013.12.001. Epub 2013 Dec 7.

Griswold MA, Jakob PM, Heidemann RM, Nittka M, Jellus V, Wang J, Kiefer B, Haase A. Generalized autocalibrating partially parallel acquisitions (GRAPPA). Magn Reson Med. 2002 Jun;47(6):1202-10. doi: 10.1002/mrm.10171.

Huang H, Zhang J, van Zijl PC, Mori S. Analysis of noise effects on DTI-based tractography using the brute-force and multi-ROI approach. Magn Reson Med. 2004 Sep;52(3):559-65. doi: 10.1002/mrm.20147.

Macovski A. Noise in MRI. Magn Reson Med. 1996 Sep;36(3):494-7. doi: 10.1002/mrm.1910360327.

Mishro PK, Agrawal S, Panda R, Abraham A. A Survey on State-of-the-Art Denoising Techniques for Brain Magnetic Resonance Images. IEEE Rev Biomed Eng. 2022;15:184-199. doi: 10.1109/RBME.2021.3055556.

Pruessmann KP, Weiger M, Scheidegger MB, Boesiger P. SENSE: sensitivity encoding for fast MRI. Magn Reson Med. 1999 Nov;42(5):952-62.

All Bruker *in vivo* animal work was approved by the institutional animal care and use committee (IACUC) or local authorities and conducted under valid study permit.

Bruker BioSpin
info@bruker.com

bruker.com

Customer Support
https://www.bruker.com/en/services/support.html

Online information
bruker.com/